The parallel calculations of fully differential cross section for transfer excitation reactions in fast proton-helium collisions

M.S. Schöffler[1], O. Chuluunbaatar[2,3], S. Houamer[4], A.G. Galstyan[5], J. Titze[1], T. Jahnke[1], L.Ph.H. Schmidt[1], Yu.V. Popov[6], A. Bulychev[2]

[1]Institut für Kernphysik, University Frankfurt, Frankfurt, Germany
[2]Joint Institute for Nuclear Research, Dubna, Russia
[3]National University of Mongolia, UlaanBaatar, Mongolia
[4]Département de physique, Faculté de Sciences, Université Ferhat Abbas, Sétif, Algeria
[5]Physics Faculty, Moscow State University, Moscow, Russia
[6]Skobeltsyn Institute of Nuclear Physics, Moscow State University, Moscow, Russia

Introduction

From an experimental point of view, single-electron transfer has at least two interesting facets. First, it can be used as a tool for spectroscopy. Energy gain spectroscopy and the related experiments in inverse kinematics which exploit the recoil ion longitudinal momentum for Q-value determination (change in the electron binding energies) give access to the energy levels of highly charged species and to energy levels that do not decay radiatively. These are difficult to access by other spectroscopic techniques. Second, the dynamics of the transfer process itself is of fundamental interest since it combines electron-electron dynamics, correlation, and questions of few-body momentum exchange.

In most of the theoretical studies the transfer into an excited state or the transfer combined with a target excitation of a second electron were neglected. Especially at higher impact energies $E_p > 100$ keV/u, where the final state determination in experiments are difficult, the influence of excitation has not been investigated. Nowadays the modern experimental technique of COLTRIMS (Cold Target Recoil Ion momentum spectroscopy) allows to measure the final electronic states in electron transfer reactions even at high impact energies.

We consider here the transfer reaction p+He $\rightarrow$ H+He$^+$ at different high proton energies and present both the experimental single differential cross sections for total excitation of the residual helium ion ($n \geq 2$), and the calculations within first Born approximation (FBA).

Experiment

For the swift collisions investigated here, the best resolution is obtained by detecting the recoil ion momentum instead of small change on the large projectile momentum. In the present experiments we have used the COLTRIMS technique to measure both the neutral projectile H_0 and the recoil ion He^+ in coincidence [1, 2]. The experiment has been performed at the 2.5 MV van de Graaff accelerator at the Institut fur Kernphysik, University of Frankfurt. We used two sets of adjustable slits to collimate the beam to a size of 0.5×0.5 mm^2 at the target. Two sets of electrostatic deflectors are placed in front and behind the target. They were used to clean the beam from charge state impurities in front of the target and to analyze the final charge state behind the target. The neutral H_0 projectiles were detected on a 40 mm position- and timesensitive multichannel plate (MCP) detector with delay line anode for position read-out [3]. The target is provided by a 2-stage supersonic gas jet. At the interaction point, the gas jet has a diameter of 1.5 mm and areal density of 5×10^{11} atoms/cm^2. The He^+ recoil ions produced in the overlap region of gas jet and projectile beam were projected with a weak electrostatic field (4.8 V/cm) onto a 80 mm position- and time-sensitive multi channel plate detector. A three-dimensional time- and space-focusing geometry was applied to maximize the resolution [4]. From the measured data, time of flight (19 μs for He^+) and position of impact, we extracted the initial three-dimensional momentum vector. We achieved an overall momentum resolution of 0.1 a.u. which was limited by the target temperature. Our spectrometer geometry and electric fields yielded 4π acceptance angle for all recoil ions with momenta below 9 a.u.

In the plane perpendicular to the beam axis, we measure the scattering angle of the projectile and the transverse momentum of the recoiling ion. By momentum conservation they must add to zero. We used this for background suppression. We deduced the scattering angle from the recoil ion transverse momentum, which has a much better momentum resolution in our setup. By gating on the different longitudinal momenta of the recoil ion, we were able to extract the scattering angles for different final electronic states [5]. The small background contribution, mainly from single ionization, has been subtracted.

Theory

Let us denote the projectile proton momentum by $\vec{p}_p$, the hydrogen momentum by $\vec{p}_H$, and the recoil-ion momentum by $\vec{K}$. We also define the transferred momentum as $\vec{q} = \vec{p}_H - \vec{p}_p$. We can deduce its approximate value using the momentum and energy conservation

$$\vec{q} + \vec{K} = 0, \tag{1}$$

$$\frac{p_p^2}{2m_p} + E_0^{He} = \frac{p_H^2}{2(m_p+1)} + \frac{K^2}{2M} + E^H + E^{ion}. \tag{2}$$

Here $\vec{k}$ is the ejected electron momentum, the proton mass $m_p = 1836.15$, the helium ion mass $M \approx 4m_p$, $E_0^{He} = -2.903724377034$ [6].

Now we choose very small scattering angles for the outgoing hydrogen ($0 \leq \theta_p \lesssim 1.5$ mrad). It leads to a practically zero ion velocity K/M in the laboratory frame during the process, and we can consider the ion like immovable. The proton velocity $\vec{v}_p = \vec{p}_p/m_p$ varies about a few a.u. for its energy of several hundredths keV. This fact allows one to neglect $K^2/2M$ and $q^2/2m_p$ after insertion of $\vec{p}_H = \vec{q}+\vec{p}_p$ into Eq. (2). As a result we obtain

$$\vec{v}_p\vec{q} = \frac{1}{2}v_p^2 + Q; \quad Q = E_0^{He} - E^H - E^{ion}, \tag{3}$$

and choose the vector $\vec{v}_p$ as z-axis; there follows the longitudinal component $q_z = v_p/2 + Q/v_p$. The transverse component of the vector is $q_\perp = (\vec{p}_H)_\perp \approx m_p v_p \theta_p$.

We have two types of single differential cross section (SDCS) for TE processes:

Theory

$$\frac{d\sigma^{(1)}}{d\theta_p} = \frac{m_p^2\theta_p}{(2\pi)} \sum_{n=2}^{n-1}\sum_{l=0}^{l}\sum_{m=-l}^{l} |T_{nlm}^{FBA}|^2 \tag{4}$$

and

$$\frac{d\sigma^{(2)}}{d\Omega_p} = \frac{m_p^2}{(2\pi)^2} \sum_{n=2}^{n-1}\sum_{l=0}^{l}\sum_{m=-l}^{l} |T_{nlm}^{FBA}|^2 \tag{5}$$

In theoretical calculations we use four trial ground-state helium wave functions. One is the loosely correlated $1s^2$ Roothaan et al (RHF) wave function [7] (no angular correlation) with a rather poor ground-state energy of $E_{He}^{RHF} = -2.8617$ a.u. Second one Silverman et al (SPM) wave function [8] includes angular correlations, but its ground energy is also far from the experiment $E_{He}^{SPM} = -2.8952$ a.u. Two another trial functions are highly correlated ones. It is given in Mitroy et al (MMW) [9] with a ground-state energy of $E_{He}^{MMW} = -2.9031$ a.u. and that of Chuluunbaatar et al (CPV) [10] with $E_{He}^{CPV} = -2.903721$ a.u. Their energies are very close to the experimental value.

We omit in short the mathematical details of description of the symmetrized matrix elements $|T_{nlm}^{FBA}|$, which are given in [11, 12]. We calculate them with use of 3D and 6D integrals.

Numerical integration details

The corresponding integrals are calculated using the adaptive subdivision algorithm, and it has a loop that contains four steps:

i) determine a new subdivision of the integration region,
ii) apply the basic rule to any new subregions,
iii) combine new results from step ii) with previous results and
iv) check for convergence.

For p-processors parallelization of above algorithm we used the Single list algorithm:

p-sect region $[a_1, b_1] \times [a_2, b_2] \times \cdots \times [a_d, b_d]$
do parallel
  apply integration rule to subregions
end do parallel
do while (error $> \epsilon$) and (number of rule evaluations $\leq N_{\max}$)
  SUBREGION SELECTION
  do parallel
    compute new subregion limits
    apply cubature rule to new subregions
  end do parallel
  do parallel
    remove old subregions from list
    add new subregions to list
    update integral approximation and error estimate
  end do parallel
end do

Our p-processors parallel calculations are approximately $0.8p$ times faster than single processor.

Results and discussion

In Fig. 1 we present experimental and theoretical SDCS1.

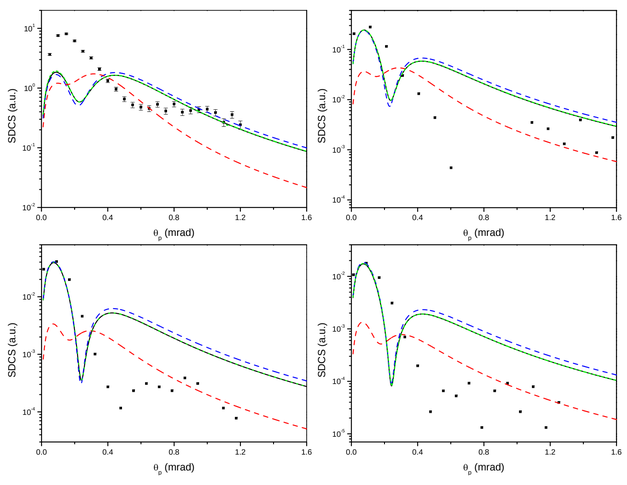

Figure 1: Experimental and theoretical data for $E_p = 300$ keV (left-top panel), $E_p = 630$ keV (right-top panel) $E_p = 1000$ keV (left-bottom panel), $E_p = 1200$ keV (right-bottom panel) p+He collisions. Full squares is the experiment, red line the RHF [7] trial helium wave function, blue line SPM [8], green line MMW [9] and black line CPV [10] practically coincide. $n = 2 + 3$.

The shape of the SDCS1 is formed by three FBA terms, one of which (OBK) provides the direct He$\rightarrow$ e+He$^+$ decay mechanism, and two others provide the double decay of the helium in the intermediate state He$\rightarrow$ 2e+He^{2+}. The absolute value of the cross sections is about 1% of that when the residual ion stays in its ground state (charge transfer, CT), and the shape in the case of helium wave functions with angular correlations has the minimum and reminds the case $n = 1$ [12]. The wave function without angular correlations fails at all. It is interesting to note, that FBA SDCS1 for CT reactions practically does not depend on the trial helium wave function, and even the simplest $1s^2$ one describes well the main peak.

We also see that $E_p \sim 500$ keV is the boundary energy when FBA still describes somehow the main peak at very small θ_p. The FBA also fails to describe the position of the minimum and the behavior of the cross section beyond it. We need to attract here the SBA or DWBA calculations.

Results and discussion

We have to work out at least computer code for 9D integration to calculate the SBA or DWBA. Such the FBA calculations of the SDCS2 are presented in [13] for $E_p = 300$ keV, but the result was about 150 times bigger than the experiment. Our correct results on the base of 9D calculations are presented for the first time in Fig. 2. They quite coincide with both 3D and 6D calculations, and the experiment ($n = 2 + 3$). See also our discussion in [14, 15].

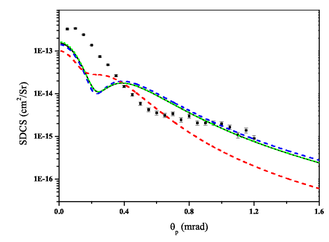

Figure 2: SDCS2 calculations versus the scattering angle θ_p at $E_p = 300$ keV. Colors of curves are the same like in Fig. 1.

Next, we calculate 9D integral with the eikonal phase-factor obtained earlier in [12]

$$T_{nlm}^{DWBA} \approx \sqrt{2}\int d^3R e^{-i\vec{R}\vec{q}} \int d^3\rho e^{i\vec{\rho}\vec{v}_p}\,\varphi_0(\rho) \int d^3r_2 \phi_{nlm}^*(\vec{r}_2)\times$$
$$e^{[-i/v_p\, f(\vec{R},\vec{\rho},\vec{r}_2)]}\left[-\frac{1}{\rho} - \frac{1}{|\vec{R}-\vec{r}_2|} + \frac{2}{R}\right]\Phi_0(\vec{R}-\vec{\rho},\vec{r}_2). \tag{6}$$

with

$$f = \ln\left[\frac{[v_p|\vec{R}-\vec{\rho}| + \vec{v}_p\cdot(\vec{R}-\vec{\rho})]^2\,[v_p|\vec{R}-\vec{r}_2| + \vec{v}_p\cdot(\vec{R}-\vec{r}_2)]}{[v_pR + \vec{v}_p\cdot\vec{R}]^2\,[v_p|\vec{R}-\vec{\rho}-\vec{r}_2| + \vec{v}_p\cdot(\vec{R}-\vec{\rho}-\vec{r}_2)]}\right].$$

This phase-factor is a part of the SBA, and can be considered like modified 4C approximation (in analogy to 3C and 6C). Results for $E_p = 300, 630, 1000$ and 1200 keV are presented in Fig. 3. We see positive evaluation of the main peak towards the experiment. However, this DWBA can not improve the situation at bigger scattering angles, and full SBA calculations are needed.

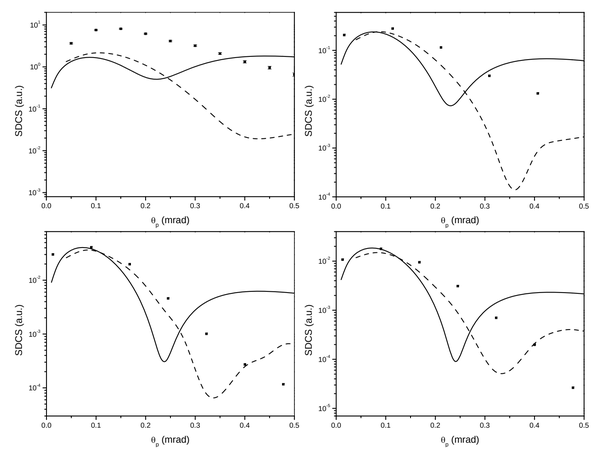

Figure 3: SDCS1 calculations versus the scattering angle θ_p. Solid line: SPM, dashed line: SPM with the 4C phase factor. $E_p = 300$ keV (left-top), $E_p = 630$ keV (right-top) $E_p = 1000$ keV (left-bottom), $E_p = 1200$ keV (right-bottom).

Conclusion

In conclusion, we present the SDCS experimental data and FBA theory for transfer excitation proton-helium collision at 300, 630, 1000 and 1200 keV/u. In calculations both $1s^2$ and highly correlated trial helium wave functions are used. The $1s^2$ wave function fails to describe the experiment, while angular correlated functions give practically coincident results and well reproduce the experiment in a vicinity of main peak. 300 keV/u results show the limit for the FBA theory. Also 3D, 6D and 9D calculations give coincident results, close to the experiment.

We modified the several standard Fortran codes for evaluate a high-dimensional integral using the adaptive subdivision method. Now they keep more data in the memory, can use the complex arithmetics and are adapted for parallel calculations.

References

1 J. Ullrich *et al.*, J. Phys. B **30**, 2917 (1997); Rep. Prog. Phys. **66**, 1463 (2003).
2 R. Dörner *et al.*, Phys. Rep. **330**, 95 (2000).
3 O. Jagutzki *et al.*, Nucl. Instrum. Meth. Phys. Res. A **477**, 244, 256 (2002).
4 R. Dörner *et al.*, Nucl. Instrum. Meth. Phys. Res. B **99**, 111 (1995).
5 M.S. Schöffler *et al.*, Phys. Rev. A **79**, 064701 (2009).
6 O. Chuluunbaatar *et al.*, J. Phys. **B 44**, L425 (2001).
7 E. Clementi and C. Roetti. Atomic Data and Nuclear Data Tables **14**, 177 (1974).
8 J.N. Silverman *et al.* J. Chem. Phys. **32**, 1402 (1960).
9 J. Mitroy *et al.*, J. Phys. B **18**, 4149 (1985).
10 O. Chuluunbaatar *et al.*, Phys. Rev. A **74**, 014703 (2006).
11 S. Houamer *et al.*, Phys. Rev. A **81**, 032703 (2010).
12 H.-K. Kim *et al.*, Phys. Rev. A **85**, 022707 (2012).
13 U. Chowdhury *et al.*, J. Phys. B **45**, 035203 (2012).
14 S. Houamer *et al.*, J. Phys. B **46**, 028001 (2013).
15 U. Chowdhury *et al.*, J. Phys. B **46**, 028002 (2013).